Supporting Information for

Crystal Engineering of co-crystal of antipyrine and 2-chlorobenzoic acid: relative energetic contributions from multipolar refinement

Aqsa Bilal[a], Arshad Mehmood[b], Sajida Noureen[a], Claude Lecomte[c,d], Maqsood Ahmed[a*]

[a]Materials Chemistry Laboratory, Institute of Chemistry, The Islamia University of Bahawalpur, Baghdad-ul-Jadeed Campus 63100, Pakistan.

[b]Department of Chemistry and Biochemistry, Texas Christian University, Fort Worth, Texas

76129, USA. [c]Universite´ de Lorraine, Laboratoire CRM2, UMR CNRS 7036, Boulevard des aiguillettes BP70239, Vandoeuvre-les-Nancy, 54506, France, and [d]CNRS, Laboratoire CRM2, UMR CNRS 7036, Boulevard des aiguillettes, BP70239, Vandoeuvre-les-Nancy, 54506, France

*Correspondence e-mail: *maqsood.ahmed@iub.edu.pk*

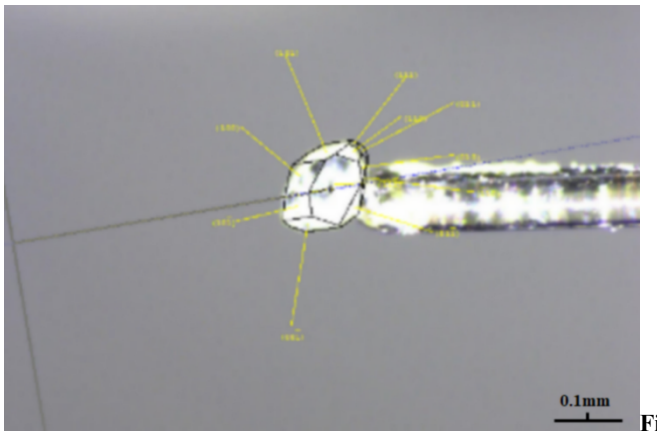

Figure S1 Crystal image of co-crystal mounted on glass needle.

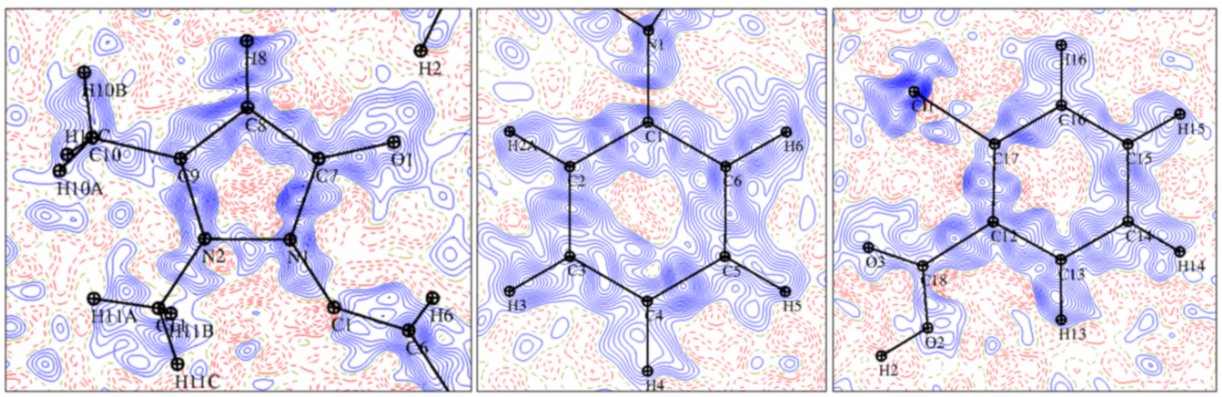

Figure S2 Residual electron density maps of molecular complex **(AN-CBA)** after IAM refinement with *MoPro* at contour level of 0.05 e Å^{-3} and with sinθ/λ=0.95 Å^{-1}.

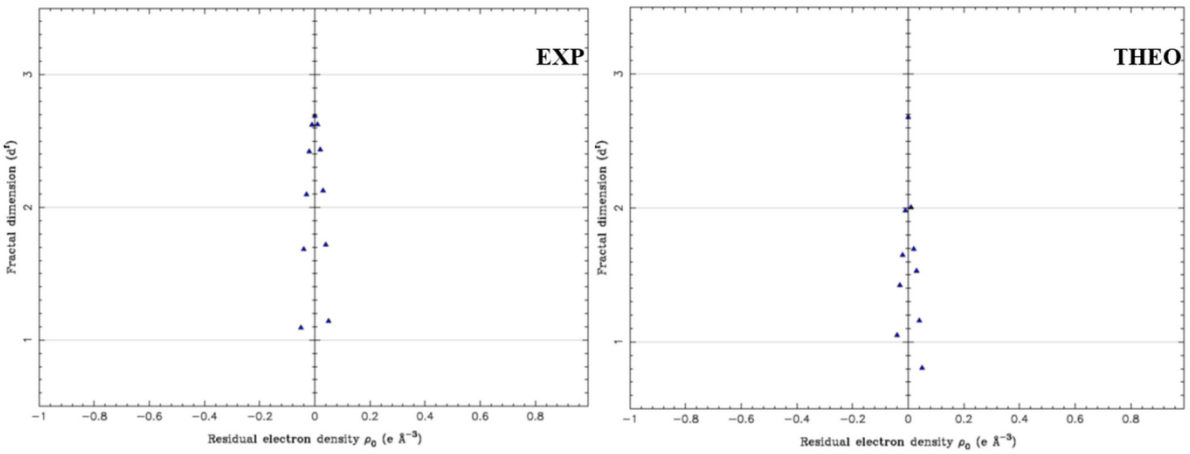

Figure S3: A fractal dimensions plot comparing the residual electron densities after experimental and theoretical ($\sin\theta/\lambda$ of 0.95 $Å^{-1}$) multipolar refinements.

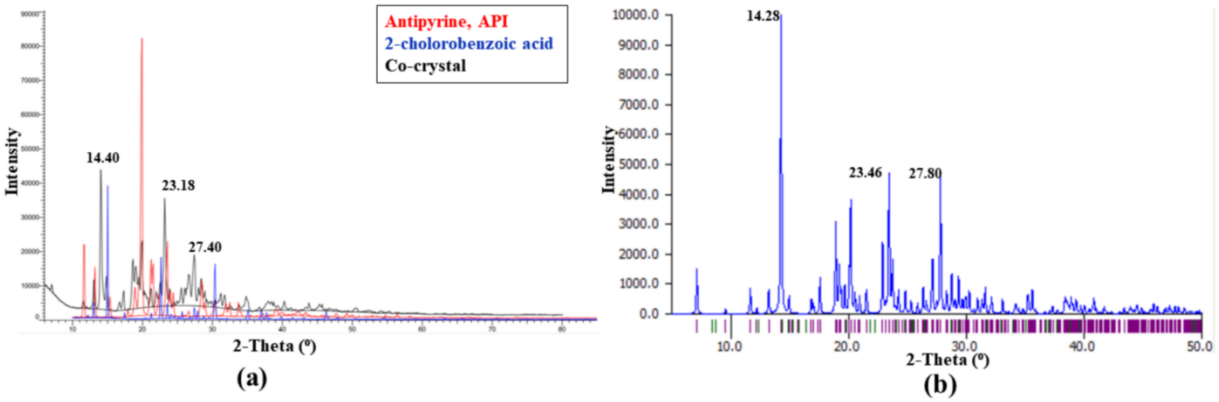

Figure S4 Powder X-ray diffraction pattern for co-crystal (**AN-CBA**), antipyrine and 2-chloro benzoic acid (a) and simulated pattern for co-crystal (b).

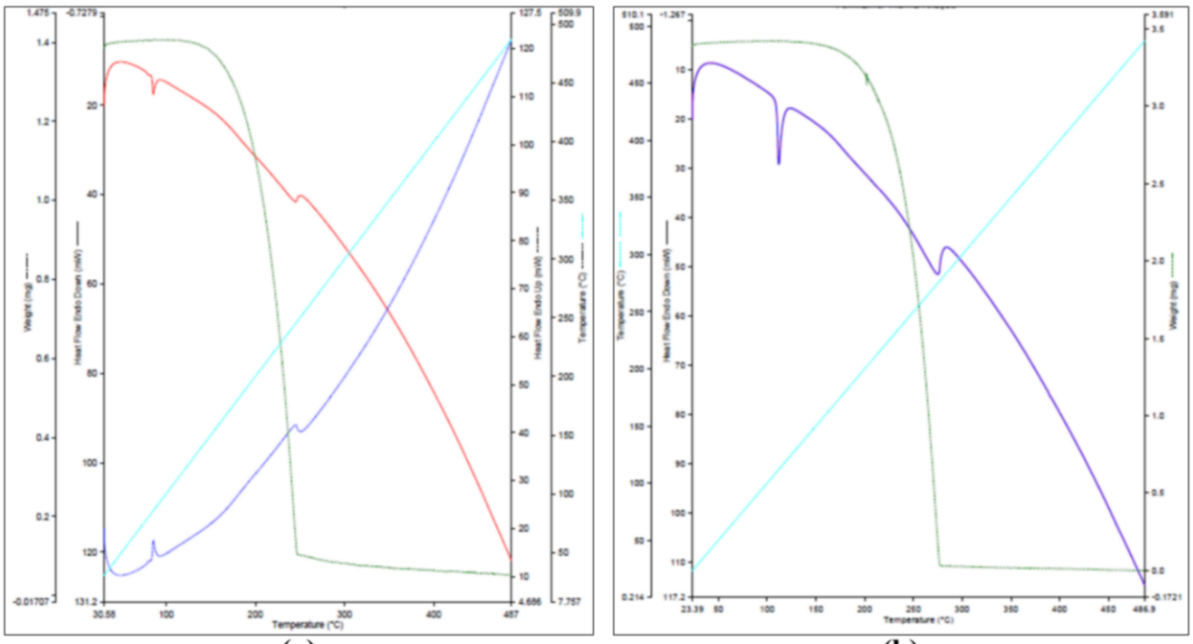

Figure S5 TGA with DSC curve of **(a)** co-crystal, **AN-CBA** and **(b)** pure antipyrine.

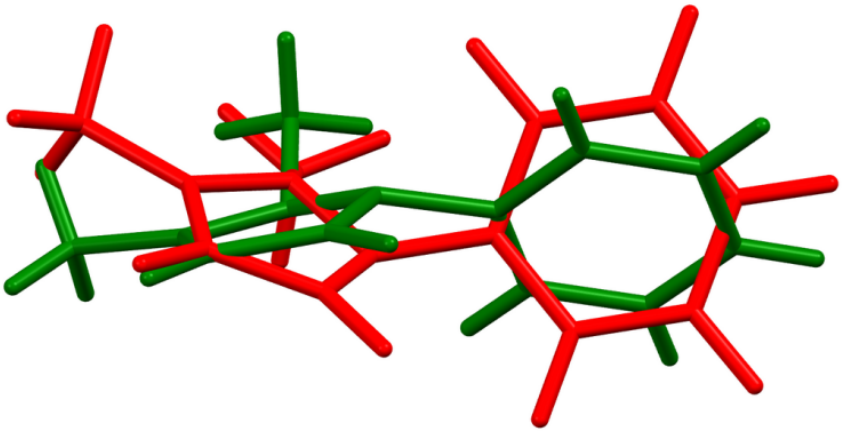

Figure S6 A structure overlay of AN moiety in cocrystal (red) and pure drug (green).

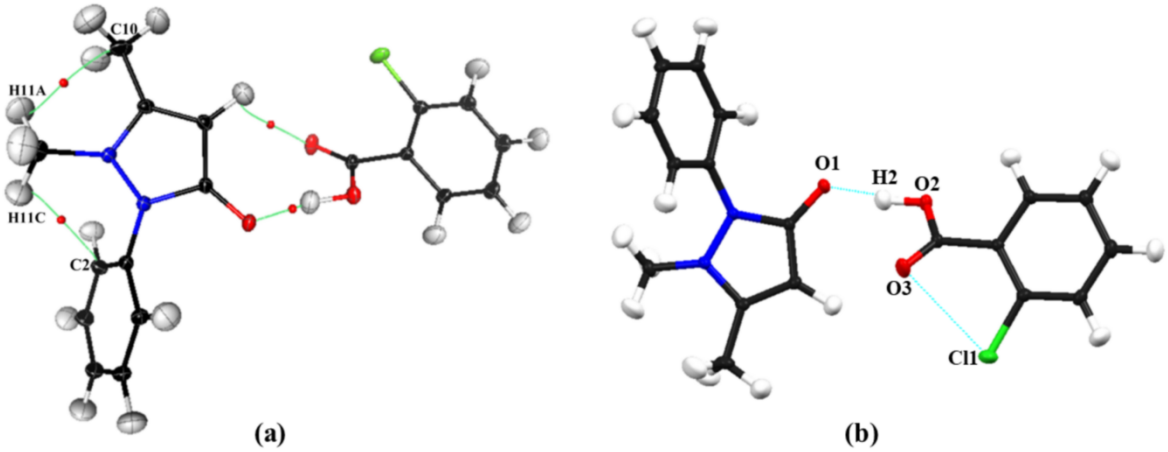

Figure S7 Influence of non-covalent interaction, C···H: (a) chalcogen bond, O3···Cl1 and (b) on molecular geometry of antipyrine in co-crystal.

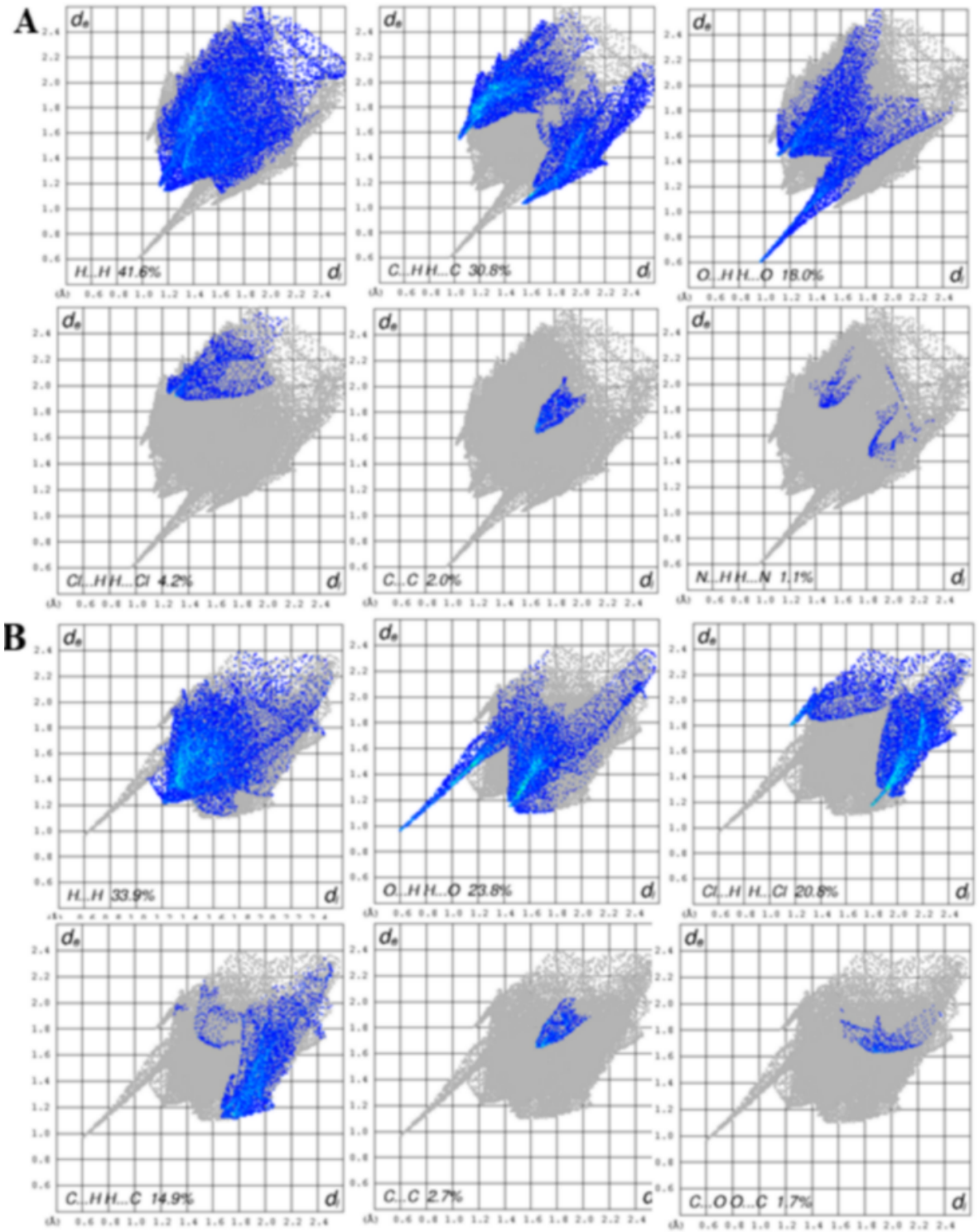

Figure S8 Fingerprint plots of antipyrine **(A)** and 2-Cholrobenzoic acid **(B)**, showing the percentage of various interactions in the co-crystal **AN-CBA**

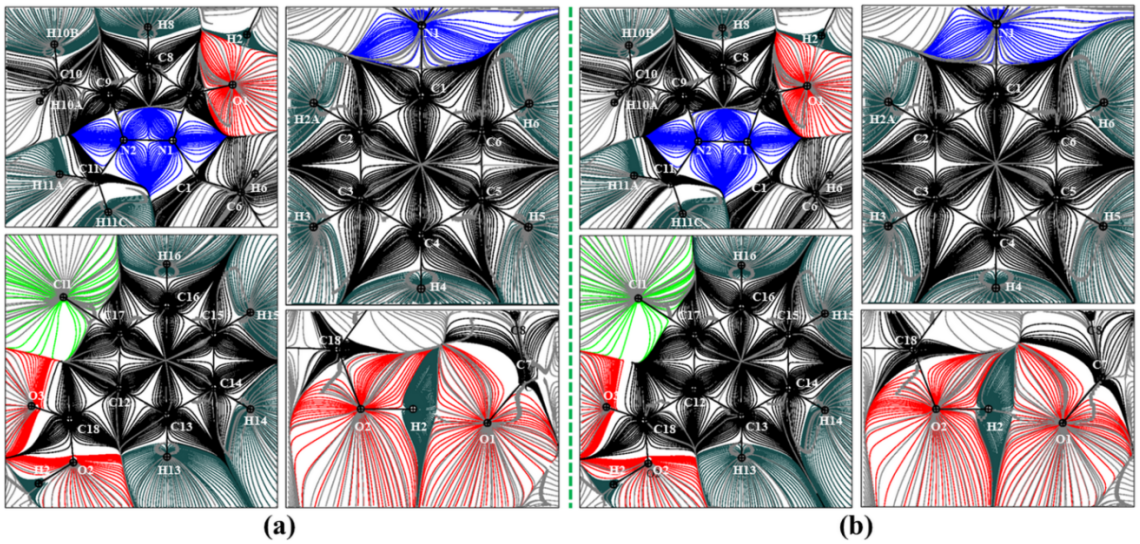

Figure S9 Gradient vector field of (a) MM_{exp} and (b) MM_{theo} model of the molecular complex **AN-CBA**, showing the zero flux surfaces forming boundaries of atomic basin of individual atoms.

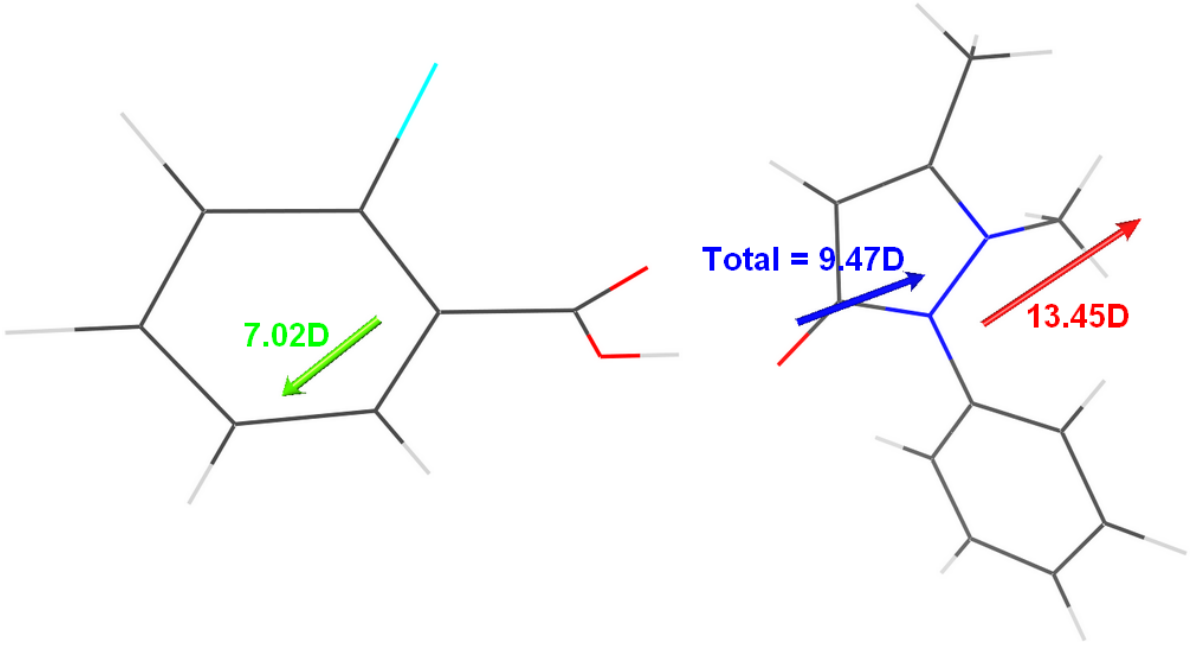

Figure S10: Dipole moment and their direction of molecular complex **(AN-CBA)**.

Table S1: The optimized and neutron bond lengths of H atoms.

No.	Bonds	$D_{optimise}$ (Å)	$D_{neutron}$ (Å)
1	O2—H2	1.04627	0.980
2	C2—H2A	1.08886	1.083
3	C3—H3	1.08998	1.083
4	C4—H4	1.08821	1.083
5	C5—H5	1.08982	1.083
6	C6—H6	1.08870	1.083
7	C8—H8	1.08040	1.083
8	C10—H10C	1.09980	1.077
9	C10— H10B	1.09304	1.077
10	C10— H10A	1.09712	1.077
11	C11— H10B	1.09634	1.077
12	C11— H10A	1.09167	1.077
13	C11— H10C	1.09265	1.077
14	C13—H13	1.08837	1.083
15	C14—H14	1.08931	1.083
16	C15—H15	1.08985	1.083
17	C16—H16	1.08872	1.083

Table S2: List of chemical constraints.

CONKAP	C2				C6	
CONKAP	C3				C5	
CONKAP	C4				C14	
CONKAP	H2A				H6	
CONKAP	H3	H4	H5	H13	H14	H15
CONKAP	H10A		H10B		H10C	
CONKAP	H11A		H11B		H11C	
AVEPVM	C2				C6	
AVEPVM	C3				C5	
AVEPVM	C4				C14	
AVEPVM	C3		C4		C13	C15
AVEPVM	H2A				H6	
AVEPVM	H3	H4	H5	H13	H14	H15
AVEPVM	H10A		H10B		H10C	
AVEPVM	H11A		H11B		H11C	
AVEPVM	H2A	H3	H8	H10A	H16	
SYMPLM mxmy			Cl1			
SYMPLM			N1			
SYMPLM mz			O1			
SYMPLM mymz			C1			
SYMPLM mz			O2			
SYMPLM			N2			
SYMPLM mymz			C2			
SYMPLM mymz			C3			
SYMPLM mz			O3			
SYMPLM mymz			C4			
SYMPLM mymz			C5			
SYMPLM mymz			C6			
SYMPLM mz			C7			
SYMPLM mz			C8			
SYMPLM mz			C9			
SYMPLM 3m			C10			
SYMPLM 3m			C11			
SYMPLM mz			C12			
SYMPLM mymz			C13			
SYMPLM mymz			C14			
SYMPLM mymz			C15			
SYMPLM mymz			C16			
SYMPLM mz			C17			
SYMPLM mz			C18			

Table S3

Crystallographic Refinement details of the **AN-CBA cocrystal** without I/σ cutoff.

Refinement	***MM (MoPro)***	***IAM (MoPro)***
Total Number of reflection measured/independent	119630/13656	
Weighting scheme	σ w^2 = ($a$sigY_o^2) where a = 1.73034	
Refinement based on	F^2	F^2
$R[F^2 > 2\sigma(F^2)]$, $wR(F^2)$, S	0.044, 0.029, 0.99	0.062, 0.101, 0.99
No. of reflections used	12342	12342
No. of parameters	804	217
$\Delta\rho_{min}$, $\Delta\rho_{max}$ (e Å^{-3})	-1.084, 0.955	-0.698, 0.756

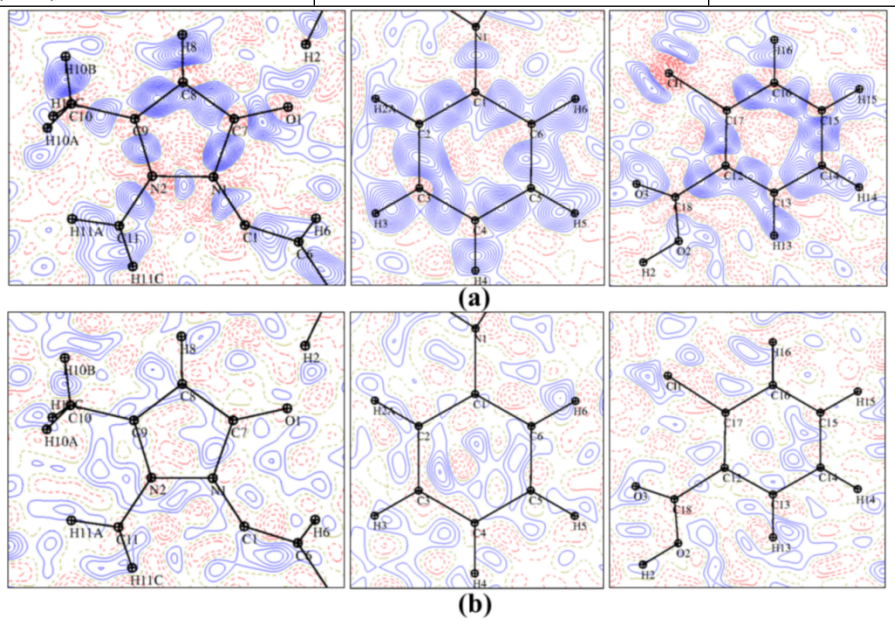

Figure S11 Residual electron density maps of molecular complex **(AN-CBA)** after (a) IAM and (b) MM_{exp} refinement with *MoPro* at contour level of 0.05 e Å^{-3} and with sinθ/λ=0.7 Å^{-1}.

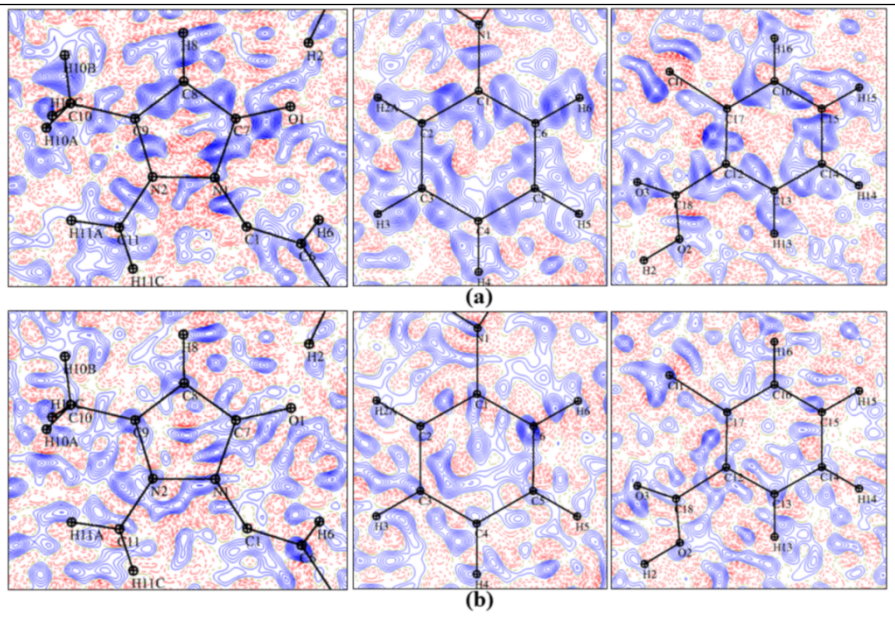

Figure S12 Residual electron density maps of molecular complex **(AN-CBA)** after (a) IAM and (b) MM_{exp} refinement with *MoPro* at contour level of 0.05 e Å^{-3} and with sinθ/λ=0.95 Å^{-}

S1. Charge density distribution

The study of topological properties reveals important information about bond type i.e. covalent, ionic, H—H interaction, Van der Waal's forces and strength of chemical bonds [1]. Topological analysis of **(I)** has been performed based on the following topological indicators i.e. the electron density, ellipticity, electrostatic potential and dipole moment. There is a very good agreement between the experimental and theoretical values that prove that the experimental model is correct. All BCPs, electron density $\rho_{BCP}(r)$, and laplacians of electron density of co-crystal have been calculated and summarized in **Table S4.** The electron density derived topological parameter of pyrazalone ring, later discussed in detail, are yet to be reported in literature.

Static deformation density [$\Delta\rho_{static}(r)$] map was plotted using *MoProViewer* software [2] and shown in **Figure S13(a).** These maps represent comparable results with characteristic accumulation of electron density both in bonding as well as lone pair regions. In particular, the loan pair around O1 and O3 is normal for carbonyl oxygen participating as acceptors of hydrogen bonds (C7=O1····H2 and C18=O3····H8). However, a sharp contrast in electron density accumulated at N1—N2 and N1—C7 in pyrazalone ring is observed in both experimental and theoretical model (table S3).

The aspherical electron density distribution observed around Cl atom in static deformation density maps is due to polar fattening effect [3, 4]; better depicted by the 3D static deformation density map as illustrated in **Figure S13(b)**.

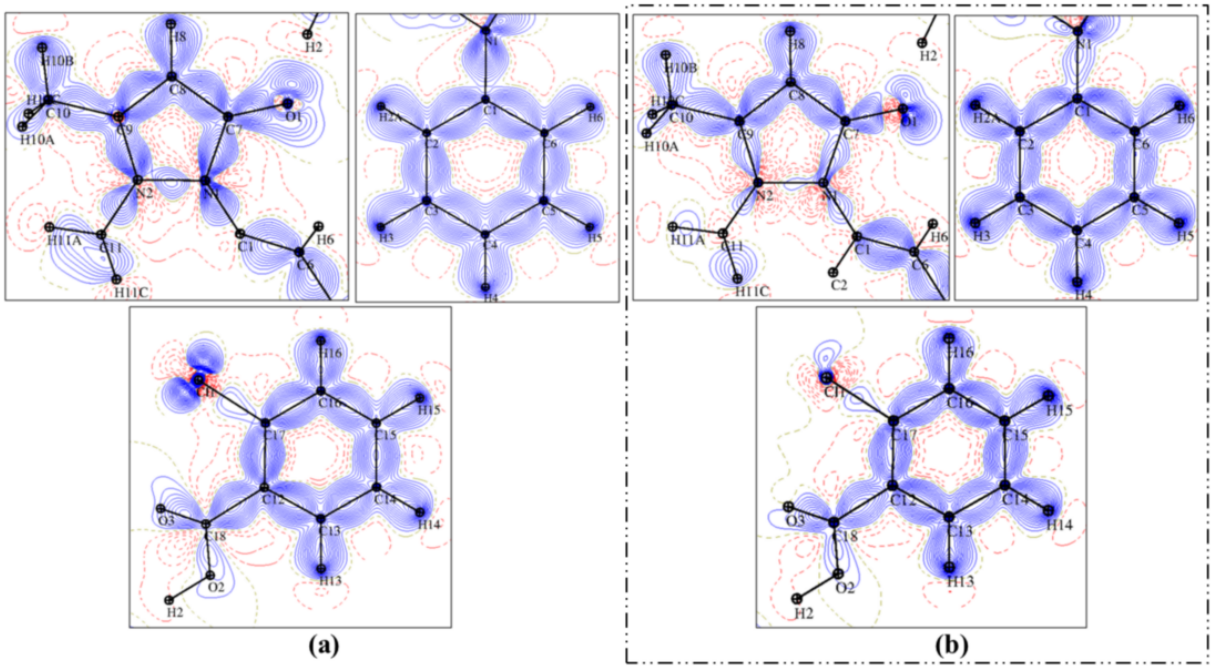

Figure S13 (a) Static deformation density maps after (a) MM_{exp} and (b) MM_{theo} refinement at contour level of 0.05 e Å^{-3}.

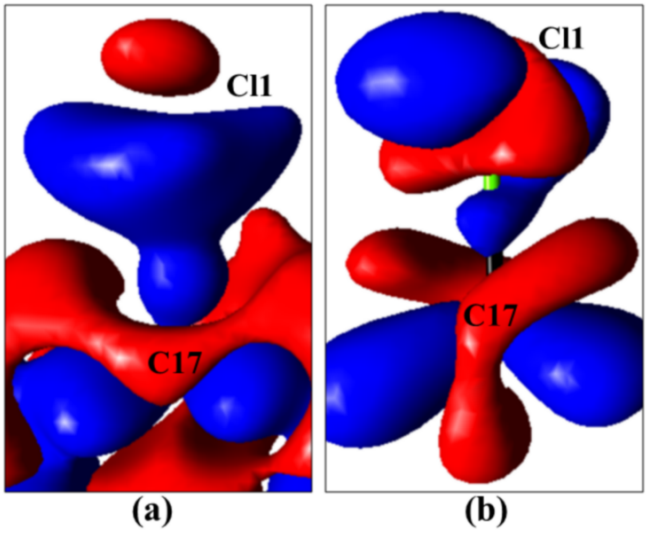

Figure S13 (b) 3D static deformation density maps of C17-Cl1 bond after (a) MM_{exp} and (b) MM_{theo} refinement at contour level of 0.05 e Å^{-3}.

Table S4

Topological properties of (3, -1) CPs in covalent interaction of **(AN-CBA):** distance (Å), electron density (e Å^{-3}), Laplacian (e Å^{-5}), Hessians eigenvalues (e Å^{-5}), and ε = ellipticity. The experimental values are given in upper line and theoretical values in lower line.

Bond	d_{12}	d_{1CP}	d_{2BCP}	$\rho_{BCP}(r)$	$\nabla^2_{BCP}(r)$	λ_1	λ_2	λ_3	ε
O3=C18	1.214	0.795	0.419	2.964	-26.860	-29.92	-25.09	28.15	0.192
	1.214	0.777	0.437	2.868	-28.059	-25.27	-22.84	20.05	0.106
O1=C7	1.257	0.805	0.452	2.684	-29.082	-23.56	-20.85	15.33	0.130
	1.257	0.784	0.473	2.557	-27.165	-21.94	-18.20	12.97	0.206
O2—C18	1.318	0.838	0.480	2.314	-27.079	-19.74	-17.99	10.65	0.097
	1.318	0.809	0.509	2.284	-21.370	-18.08	-16.59	13.30	0.090
N1—N2	1.392	0.692	0.700	2.222	-4.196	-18.44	-16.15	30.39	0.141
	1.392	0.699	0.693	2.015	2.754	-16.31	-12.72	31.78	0.283
C8—C9	1.371	0.674	0.698	2.216	-18.901	-16.84	-12.80	10.74	0.315
	1.371	0.644	0.727	2.095	-16.388	-15.75	-11.58	10.94	0.360
C12—C13	1.401	0.714	0.687	2.156	-18.936	-16.42	-13.42	10.91	0.224
	1.401	0.708	0.693	2.061	-16.281	-15.56	-12.37	11.65	0.258
C13—C14	1.392	0.706	0.685	2.155	-18.765	-15.44	-13.41	10.08	0.152
	1.392	0.701	0.690	1.993	-15.259	-14.68	-11.94	11.36	0.229
C3—C4	1.393	0.708	0.686	2.154	-18.652	-15.38	-13.37	10.10	0.151
	1.393	0.698	0.695	2.173	-18.040	-16.58	-13.70	12.24	0.210
C4—C5	1.395	0.687	0.709	2.148	-18.519	-15.34	-13.32	10.14	0.151
	1.395	0.694	0.702	2.077	-16.700	-15.60	-13.04	11.93	0.197
C1—C2	1.395	0.707	0.688	2.141	-18.148	-16.00	-13.11	10.96	0.220
	1.395	0.712	0.683	2.092	-17.120	-16.14	-12.91	11.93	0.250
C1—C6	1.396	0.707	0.689	2.138	-18.082	-15.97	-13.09	10.98	0.220
	1.396	0.713	0.683	2.176	-18.312	-16.91	-13.63	12.23	0.241
C12—C17	1.402	0.712	0.690	2.137	-17.857	-16.62	-12.72	11.48	0.306
	1.402	0.692	0.711	2.005	-15.068	-14.86	-11.94	11.73	0.245

C2—C3	1.393	0.694	0.700	2.133	-18.613	-16.06	-13.11	10.56	0.225
	1.393	0.701	0.692	1.974	-14.777	-14.51	-12.05	11.78	0.204
C16—C17	1.394	0.696	0.698	2.132	-17.738	-16.18	-12.81	11.25	0.263
	1.394	0.685	0.709	1.968	-14.516	-14.51	-11.58	11.57	0.253
C5—C6	1.394	0.700	0.694	2.130	-18.522	-16.03	-13.08	10.58	0.226
	1.394	0.692	0.702	1.977	-14.736	-14.52	-12.06	11.84	0.204
N2—C9	1.363	0.833	0.531	2.120	-16.174	-15.75	-14.21	13.78	0.109
	1.363	0.790	0.573	1.980	-12.862	-14.61	-12.00	13.75	0.218
N1—C7	1.394	0.824	0.570	2.109	-18.386	-16.47	-13.93	12.01	0.183
	1.394	0.803	0.591	1.834	-10.295	-13.40	-10.90	14.00	0.230
C14—C15	1.394	0.697	0.697	2.103	-17.829	-15.02	-13.10	10.29	0.147
	1.394	0.692	0.702	2.054	-16.258	-15.32	-12.53	11.58	0.223
C15—C16	1.392	0.683	0.709	2.090	-17.623	-15.51	-12.98	10.87	0.196
	1.392	0.693	0.699	2.100	-16.982	-16.02	-12.70	11.74	0.261
C7—C8	1.422	0.766	0.657	2.016	-16.826	-14.61	-11.73	9.51	0.245
	1.422	0.753	0.670	1.964	-14.364	-14.41	-11.35	11.39	0.270
N1—C1	1.421	0.872	0.549	1.857	-11.686	-12.42	-11.38	12.12	0.092
	1.421	0.803	0.618	1.736	-8.231	-12.72	-10.95	15.44	0.162
C12—C18	1.499	0.742	0.757	1.824	-14.975	-13.71	-11.85	10.59	0.157
	1.499	0.737	0.762	1.674	-11.000	-11.77	-10.43	11.20	0.129
C8—H8	1.080	0.739	0.342	1.824	-17.836	-17.74	-16.67	16.57	0.065
	1.080	0.703	0.378	1.735	-14.743	-15.95	-14.89	16.10	0.071
C6—H6	1.089	0.739	0.350	1.820	-16.887	-17.50	-16.89	17.51	0.036
	1.089	0.716	0.373	1.808	-15.488	-16.81	-16.06	17.38	0.047
C2—H2A	1.089	0.739	0.350	1.820	-16.873	-17.49	-16.89	17.51	0.036
	1.089	0.729	0.360	1.818	-15.650	-17.38	-16.48	18.21	0.055
C16—H16	1.089	0.736	0.353	1.802	-15.961	-17.28	-16.81	18.13	0.028
	1.089	0.719	0.370	1.748	-14.551	-15.91	-15.76	17.12	0.010
C13—H13	1.088	0.729	0.360	1.793	-15.946	-16.42	-16.34	16.81	0.005
	1.088	0.721	0.367	1.794	-15.532	-16.57	-16.09	17.13	0.030
C5—H5	1.090	0.730	0.360	1.791	-15.875	-16.76	-15.90	16.79	0.054
	1.090	0.726	0.364	1.826	-15.548	-17.33	-16.50	18.28	0.051
C3—H3	1.090	0.730	0.360	1.791	-15.864	-16.75	-15.90	16.79	0.054
	1.090	0.719	0.371	1.766	-14.411	-16.37	-15.73	17.69	0.040
C4—H4	1.088	0.721	0.367	1.745	-14.782	-16.01	-15.29	16.51	0.047
	1.088	0.712	0.377	1.740	-14.375	-15.89	-15.25	16.77	0.042
C15—H15	1.090	0.723	0.367	1.742	-15.044	-16.16	-15.37	16.49	0.051
	1.090	0.706	0.384	1.741	-14.310	-15.75	-14.95	16.38	0.054
C14—H14	1.089	0.722	0.368	1.742	-14.721	-15.97	-15.25	16.50	0.047
	1.089	0.730	0.359	1.793	-15.567	-17.08	-16.13	17.63	0.059
N2—C11	1.458	0.859	0.599	1.723	-11.589	-11.72	-10.67	10.80	0.099
	1.458	0.830	0.628	1.570	-5.352	-10.84	-9.61	15.09	0.128
C10—H10B	1.093	0.726	0.367	1.720	-13.599	-15.70	-15.11	17.22	0.039
	1.093	0.705	0.388	1.676	-12.645	-14.68	-14.49	16.52	0.013
C10—H10A	1.097	0.729	0.369	1.709	-13.320	-15.55	-14.96	17.19	0.039
	1.097	0.721	0.377	1.716	-13.221	-15.31	-15.24	17.33	0.004

O2—H2	1.046	0.825	0.221	1.709	-18.778	-25.09	-24.95	31.27	0.006
	1.046	0.795	0.252	1.616	-10.997	-20.84	-20.83	30.67	0.000
C10—H10C	1.100	0.730	0.370	1.702	-13.143	-15.41	-14.90	17.16	0.034
	1.100	0.723	0.377	1.742	-13.750	-15.75	-15.38	17.38	0.024
C9—C10	1.483	0.721	0.762	1.693	-10.606	-11.90	-10.83	12.12	0.099
	1.483	0.784	0.699	1.758	-11.467	-12.27	-10.86	11.66	0.130
C11—H11A	1.092	0.785	0.307	1.571	-15.867	-15.67	-13.50	13.31	0.160
	1.092	0.727	0.365	1.806	-15.318	-17.13	-16.51	18.33	0.038
C11—H11C	1.093	0.786	0.307	1.568	-15.794	-15.62	-13.48	13.30	0.158
	1.093	0.717	0.376	1.711	-13.820	-15.91	-15.13	17.23	0.052
C11—H11B	1.096	0.788	0.309	1.558	-15.532	-15.47	-13.35	13.29	0.159
	1.096	0.730	0.366	1.799	-14.252	-16.82	-16.45	19.02	0.023
Cl1—C17	1.729	0.982	0.747	1.308	-1.876	-7.77	-7.01	12.91	0.108
	1.729	0.986	0.743	1.265	-0.449	-7.11	-6.20	12.87	0.147

A graphical representation of BCP of co-crystal at all (3, -1) critical points (**Figure S14**) reveal the dissimilar positioning of the bond critical points for homonuclear and heteronuclear bonds: Position of BCPs in C—C and N—N bonds is at the middle of bond whereas BCPs of C—H, C—N and C—O bonds tend to shift towards the electropositive atoms. The carboxyl C—O bond (C18—O2; 2.314/2.284 $eÅ^{-3}$) exhibits low electron density accumulation compared to O3=C18 and O1=C7 bonds which conform that electron density is more concentrated at carbonyl functional group than other C—O bonds. The N—C bonds in pyrazolone ring exhibit different electron densities ranging from 2.120/1.980 $eÅ^{-3}$ to 1.723/1.570 $eÅ^{-3}$ (experimental/theoretical) which is comparable with literature[5-10], > 2.2 ± 0.2 $eÅ^{-3}$. Out of all N—C interactions, the N1—C7 bond has the higher value of electron density owing to the neighbouring O1 atom while the higest density accumulation is observed at N2—C9 bond due covelenty bonded electron donating C10-methyl group; resulting density depleation at neighbouring covalent bond. Additionally, the electron density contained by C—H bond in benzene rings is higher as compared to that of C—H bond in methyl group. Among all the homonuclear bonds, the N1—N2 bond in pyrazolone ring has maximum comparable theoretical and experimental electron density of 2.222/2.015 $eÅ^{-3}$. This concludes a higher concentration of electron density in N—N bonds compared to C—C bonds but still lower than the C=O and C—O heteroatomic bonds.

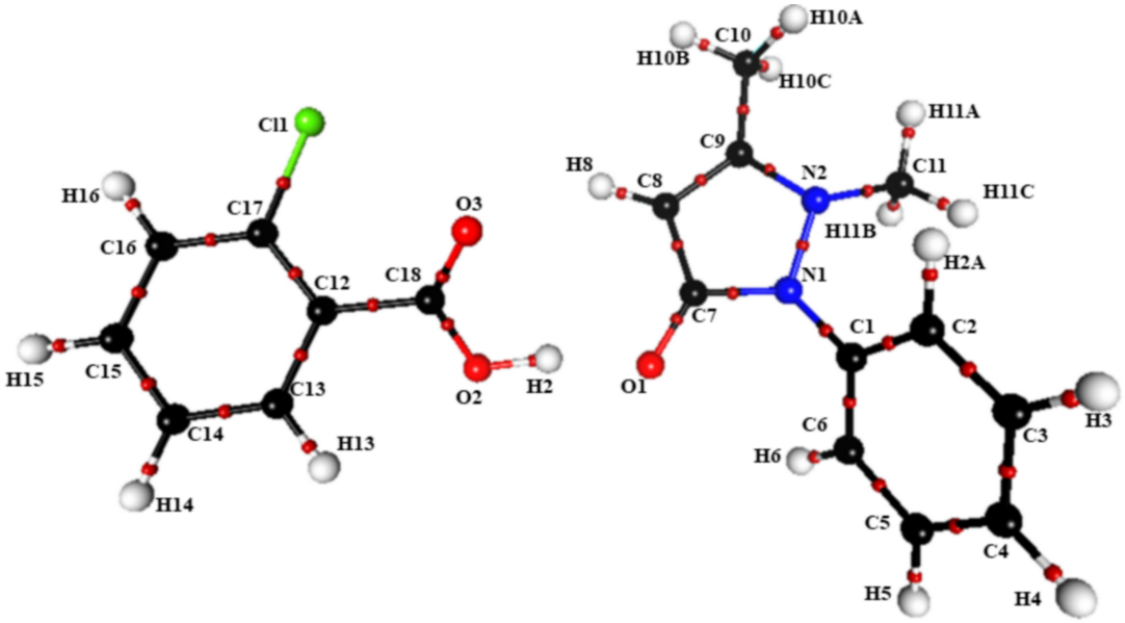

Figure S14 A view of co-crystal showing the covalent bond critical point with atom numbering scheme.

Laplacian of electron density $\nabla^2_{BCP}(r)$ as shown in **Figure S15** portray well correlated charge density concentrated and depleted regions in experimental and theoretical model which defines the electrophilic and nucleophilic sites of attacking in the various systems [11]. The negative laplacian of electron density observed at carbonyl functional group (O3=C18; -26.86/-28.06 $eÅ^{-5}$ and O1=C7; -29.08/-27.17 $eÅ^{-5}$; experimental/theoretical) is higher than carboxyl O2—C8 (-27.08/-21.37 $eÅ^{-5}$) and hydroxyl group (O2—H2; -18.78/-10.10 $eÅ^{-5}$). Additionally, the topological difference of experimental and theoretical charge density especially laplacian of polar bond is evident in table 3, not surprising as the anisotropic displacement parameters are not taken into account for the theoretical model. The carbon atom bonded to heavy atom (Cl1—C17) has laplacian of -1.88/-0.45 $eÅ^{-5}$, indicating that it contains much lower charge density accumulation at BCP than other bonds. The C—C bond of aromatic ring exhibits strongest negative laplacian of electron density (-18.94/-16.28 to -17.62/-16.98 $eÅ^{-5}$) which is consistent with aromatic delocalized bonding, as expected. Nevertheless the laplacian of electron value for N1—N2 bond is the smallest among all the bonds, at -4.20/2.75 $eÅ^{-5}$, indicating that charge concentration at this bond is lowest compared to other bonds and this noteworthy difference is due to the neighbouring benzene ring and methyl group. The negative values of $\nabla^2\rho$ (as tabulated in table 3) are a sign of the expected shared shell (covalent) character of all bonding interactions in co-crystal.

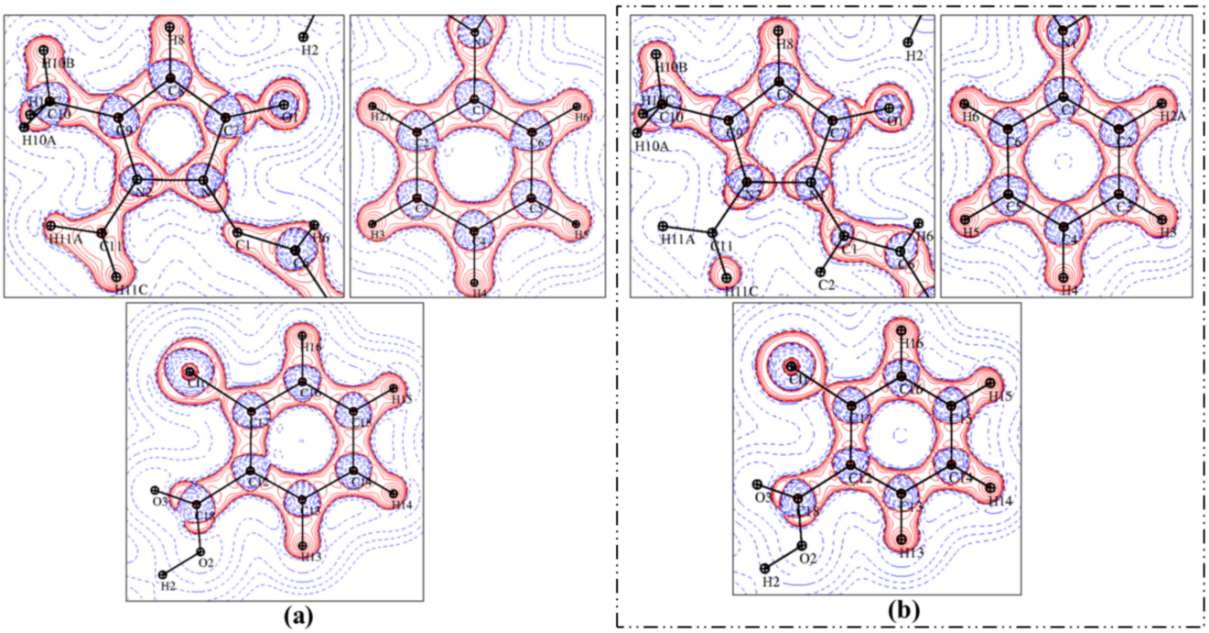

Figure S15 Laplacian maps after (a) MM_{exp} and (b) MM_{theo} refinement at contour level of 0.05 e Å^{-3}.

Bond ellipticity [$\varepsilon = \lambda_1 / \lambda_2 - 1$] measures the extent of privileged charge accretion in a plane vertical to the bond path [11]. Thus it gives an insight into the symmetric nature of electron density at BCPs and bonding nature, sigma and pi character of the bond [12, 13]. Bonds with cylindrical symmetry have ε=0 but this value is greater than 0 if a double bond is present. According to Bader, charge density prefers to accumulate more in the plane of ring than in the π-plane. Therefore in case of homonucler bonds of the ring (C—C and N—N), the C8—C9, C16—C17 and N1—N2 have ellipticity of 0.315/0.360, 0.263/0.253, and 0.141/0.283 (experimental/theoretical), depicting that the ε value is relatively higher than carbonyl bonds. Furthermore, N1—C7 bond has ε value of 0.183/0.230, which is higher than all other N—C bonds in pyrazalone ring. As for C—H bonds the ellipticity value lies in 0.005/0.030-0.160/0.038 range. The caobonyl group (O3=C18 and O1=C7) with ellipticity of 0.192/0.106 and 0.130/0.206 shows an elevation in ellipticity compared to O2—C18 bond (0.097/0.090), indicating deformation or double bond. However amongst all the bond, the O2—H1 hydroxyl bond has the smallest ε value, 0.006/0.000.

Table S5

Topological properties of (3, -1) CPs in intermolecular interaction of the **AN-CBA:** distance (Å), electron density (e Å^{-3}), Laplacian (e Å^{-5}), Hessians eigenvalues (e Å^{-5}), ε = ellipticity, G_{CP} = bond kinetic-energy density (kJ mol^{-1} Bhor^{-3}) and V_{CP} = bond potential-energy density (kJ mol^{-1} Bhor^{-3}). Experimental and Theoretical values are given in blue and red, respectively.

Interactions	d_{12}	d_{1CP}	d_{2BCP}	ρ_{BCP} (r)	$\nabla^2\rho$ (BCP)	λ_1	λ_2	λ_3	ε	G_{CP}	V_{CP}
O2—H2····O1	1.513	0.426	1.058	0.426	5.878	-2.96	-2.93	11.77	0.009	182.14	-204.17
	1.513	0.485	1.028	0.410	5.857	-2.77	-2.75	11.38	0.008	177.01	-194.49
C10—H10A····C8^{i}	2.581	1.027	1.614	0.058	0.759	-0.18	-0.13	1.06	0.402	16.51	-12.35
	2.581	1.032	1.605	0.059	0.779	-0.17	-0.12	1.07	0.409	16.95	-12.69
C14—H14····O1^{ii}	2.320	0.923	1.399	0.057	1.162	-0.20	-0.20	1.56	0.007	23.74	-15.84
	2.320	0.928	1.397	0.059	1.163	-0.22	-0.22	1.61	0.012	23.95	-16.22
C8—H8····O2^{iii}	2.662	1.210	1.488	0.051	0.752	-0.17	-0.16	1.08	0.080	15.86	-11.24
	2.662	1.223	1.483	0.045	0.694	-0.15	-0.13	0.97	0.141	14.39	-9.89
C8—H8····O3	2.704	1.233	1.500	0.043	0.628	-0.15	-0.12	0.90	0.209	13.05	-9.00
	2.704	1.233	1.507	0.040	0.613	-0.13	-0.12	0.86	0.149	12.60	-8.51
C13····C8	3.326	1.637	1.721	0.041	0.467	-0.08	-0.01	0.56	6.900	9.99	-7.26
	3.326	1.648	1.704	0.042	0.484	-0.08	-0.02	0.58	3.110	10.37	-7.57
C4—H4····C6^{iv}	2.693	1.097	1.636	0.039	0.539	-0.11	-0.07	0.72	0.516	11.19	-7.70
	2.693	1.099	1.625	0.040	0.562	-0.10	-0.07	0.73	0.324	11.65	-7.99
C10—H10C····O2^{v}	2.867	1.297	1.628	0.037	0.519	-0.11	-0.04	0.67	1.770	10.73	-7.32
	2.867	1.255	1.633	0.035	0.513	-0.10	-0.04	0.66	1.377	10.51	-7.05
C10—H10B····O3^{v}	2.926	1.293	1.687	0.035	0.489	-0.08	-0.06	0.63	0.261	10.07	-6.83
	2.926	1.296	1.686	0.032	0.466	-0.07	-0.05	0.58	0.305	9.49	-6.28
C10—H10C····O1^{v}	2.542	1.004	1.543	0.035	0.731	-0.12	-0.09	0.94	0.268	14.44	-8.98
	2.542	1.019	1.532	0.033	0.721	-0.10	-0.08	0.90	0.284	14.15	-8.67
C13—H13····O2^{ii}	2.615	1.090	1.539	0.034	0.613	-0.12	-0.11	0.84	0.102	12.25	-7.81
	2.615	1.111	1.528	0.034	0.603	-0.11	-0.11	0.82	0.001	12.06	-7.69
C2—H2A····C12^{i}	2.856	1.195	1.709	0.033	0.429	-0.08	-0.05	0.57	0.523	8.83	-5.97
	2.856	1.197	1.701	0.032	0.442	-0.07	-0.05	0.56	0.429	9.04	-6.04
C2—H2A····O3^{i}	2.633	1.042	1.592	0.031	0.635	-0.10	-0.08	0.81	0.183	12.51	-7.73
	2.633	1.056	1.578	0.030	0.623	-0.09	-0.06	0.78	0.473	12.24	-7.50
C3—H3····C16^{i}	2.963	1.189	1.824	0.030	0.401	-0.07	-0.04	0.50	0.963	8.18	-5.43
	2.963	1.174	1.799	0.030	0.422	-0.06	-0.02	0.50	1.942	8.56	-5.62
C11—H11C····C5	3.076	1.290	1.800	0.029	0.312	-0.08	-0.05	0.44	0.632	6.51	-4.53
	3.076	1.238	1.847	0.023	0.337	-0.06	-0.04	0.43	0.398	6.69	-4.21
Cl1····H14^{v}	3.218	1.405	1.853	0.028	0.347	-0.08	-0.06	0.49	-0.06	0.49	-0.06
	3.218	1.405	1.866	0.030	0.370	-0.08	-0.06	0.50	-0.06	0.50	-0.06
C10—H10A····O3	2.761	1.177	1.604	0.024	0.448	-0.07	-0.07	0.59	0.025	8.78	-5.36
	2.761	1.210	1.583	0.025	0.432	-0.07	-0.06	0.56	0.251	8.51	-5.25
Cl1····H3^{i}	3.280	1.417	1.905	0.022	0.283	-0.06	-0.05	0.39	0.110	5.66	-3.63
	3.280	1.409	1.921	0.024	0.309	-0.06	-0.04	0.41	0.279	6.26	-4.10
Cl1····H16^{vi}	2.987	1.120	1.878	0.021	0.395	-0.05	-0.05	0.50	0.032	7.67	-4.56

	2.987	1.115	1.881	0.024	0.426	-0.06	-0.06	0.55	0.006	8.38	-5.15
C15—H15····C3	3.140	1.298	1.892	0.018	0.275	-0.05	-0.03	0.36	0.730	5.39	-3.29
	3.140	1.321	1.879	0.020	0.278	-0.05	-0.02	0.35	1.045	5.51	-3.44
C6—H6····C16	3.229	1.348	1.900	0.017	0.233	-0.04	-0.02	0.29	0.633	4.59	-2.83
	3.229	1.353	1.902	0.016	0.223	-0.03	-0.02	0.27	0.984	4.35	-2.63
Cl1····Cl1^{vi}	4.186	2.093	2.093	0.011	0.149	-0.02	-0.01	0.18	1.959	2.87	-1.68
	4.190	2.095	2.095	0.015	0.190	-0.03	-0.01	0.23	1.267	3.73	-2.28

Symmetry codes: (i) -*x*+1, *y*-1/2, -*z*+1/2; (ii) -*x*+1, -*y*, -*z*+1; (iii) –*x*+1, -*y*+1, -*z*+1; (iv) -*x*, *y*+1/2, -*z*+1/2; (v) *x*, *y*-1, *z*; (vi) -*x*+2, -*y*+1, -*z*+1.

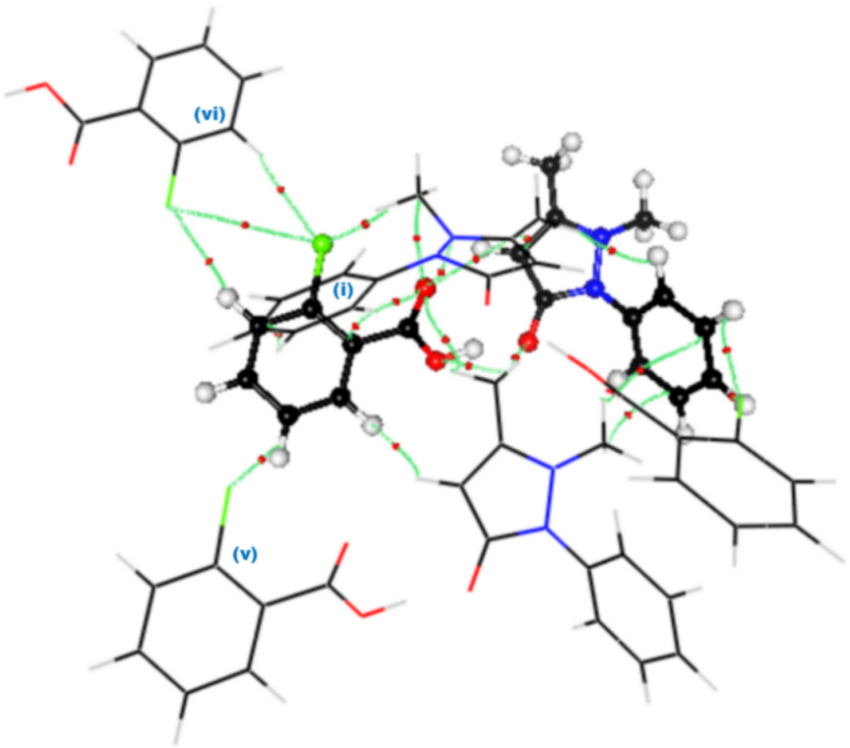

Figure S16: A view of the reference dimer in Bold (AN-CBA) surrounded by a cluster of neighbouring molecules, showing the intermolecular bond paths (green lines) and critical points (red dots) with Cl1 atom. symmetry codes are as in the man text.

Table S6

Valance population of AN and CBA moiety along with electrostatic potential of experimental and theoretical AN-CBA.

ATOMS	AN_EXP	AN_THEO	ATOMS	CBA_EXP	CAB_THEO
N1	5.19213	5.04441	Cl1	7.10304	7.1988
O1	6.39196	6.22623	O2	6.39553	6.21893
C1	4.06782	4.02175	H2	0.60546	0.70887
N2	5.20049	5.02377	O3	6.13726	6.04038
C2	4.01798	4.05285	C12	3.92065	3.9644
H2A	0.88305	0.91551	C13	4.24215	4.07078
C3	4.26912	4.053	H13	0.81387	0.90052
H3	0.81395	0.93076	C14	4.07131	4.06194
C4	4.07122	4.08872	H14	0.81401	0.8881
H4	0.81385	0.91503	C15	4.02533	4.08453
C5	4.26905	4.06063	H15	0.81387	0.92675
H5	0.81392	0.9368	C16	4.09493	4.02892
C6	4.01818	4.05622	H16	0.8715	0.91707
H6	0.883	0.92493	C17	4.10221	4.00001
C7	4.13507	4.12201	C18	4.07021	4.11504
C8	4.21706	3.81711			
H8	0.79375	0.89695			
C9	3.61309	4.18632			
C10	4.3365	3.95701			
H10A	0.88165	0.93274			
H10B	0.88156	0.94347			
H10C	0.88164	0.93885			
C11	4.70046	4.04128			
H11A	0.59078	0.92378			
H11B	0.59081	0.95399			
H11C	0.59088	0.91081			
Total	**71.91897**	**71.87493**		**52.08133**	**52.12504**

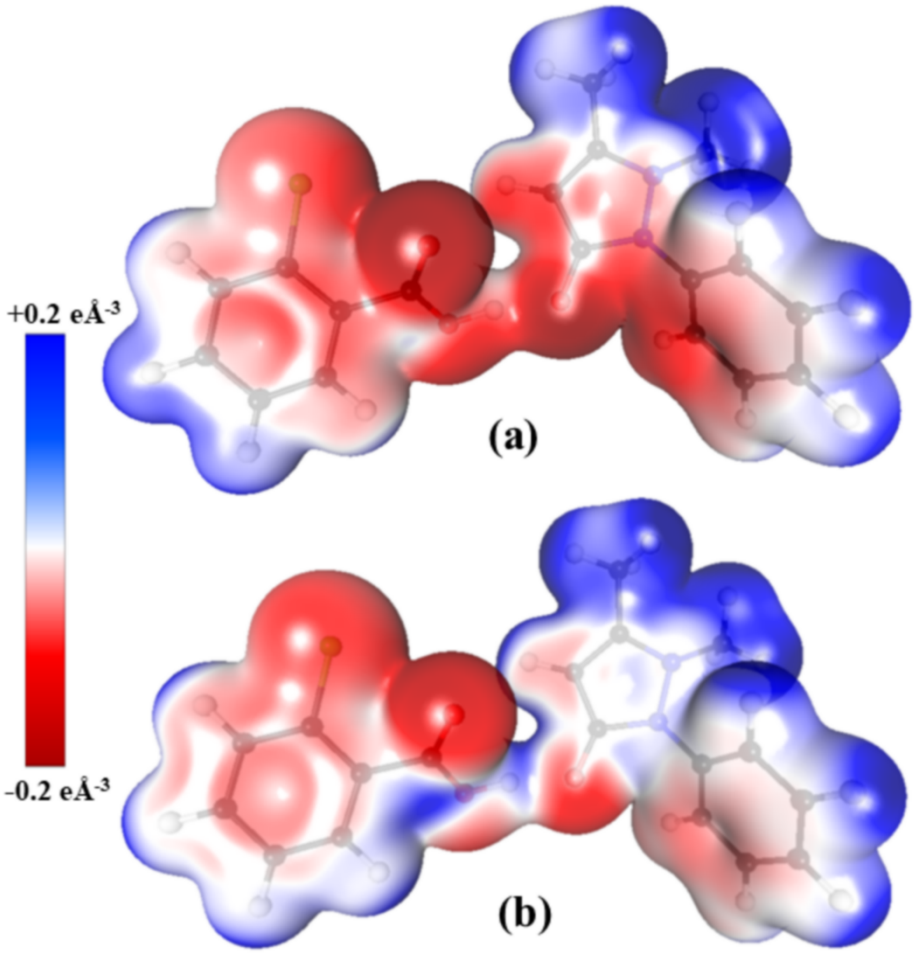

Figure S17: Electrostatic potential of co-crystal (AN-CBA) after multipolar refinement generated at isosurface value of 0.05 e/Å^3, (a) experimental and (b) theoretical.

References

1. P. S. V. Kumar, V. Raghavendra and V. Subramanian, *Journal of Chemical Sciences*, 2016, **128**, 1527-1536.
2. B. Guillot, 2012.
3. V. R. Hathwar, R. G. Gonnade, P. Munshi, M. M. Bhadbhade and T. N. Guru Row, *Crystal Growth & Design*, 2011, **11**, 1855-1862.
4. V. R. Hathwar and T. N. Guru Row, *Crystal Growth & Design*, 2011, **11**, 1338-1346.
5. A. Owczarzak and M. Kubicki, *Crystals*, 2018, **8**, 132.
6. M. Gryl, S. Cenedese and K. Stadnicka, *The Journal of Physical Chemistry C*, 2015, **119**, 590-598.
7. B. Fournier, E.-E. Bendeif, B. Guillot, A. Podjarny, C. Lecomte and C. Jelsch, *Journal of the American Chemical Society*, 2009, **131**, 10929-10941.
8. C. Kalaiarasi, M. S. Pavan and P. Kumaradhas, *Acta Crystallographica Section B: Structural Science, Crystal Engineering and Materials*, 2016, **72**, 775-786.
9. M. Gryl, A. Krawczuk-Pantula and K. Stadnicka, *Acta Crystallographica Section B: Structural Science*, 2011, **67**, 144-154.
10. J. Hey, D. Leusser, D. Kratzert, H. Fliegl, J. M. Dieterich, R. A. Mata and D. Stalke, *Physical Chemistry Chemical Physics*, 2013, **15**, 20600-20610.
11. C. Gatti, V. Saunders and C. Roetti, *The Journal of chemical physics*, 1994, **101**, 10686-10696.
12. C. Silva Lopez and A. R de Lera, *Current Organic Chemistry*, 2011, **15**, 3576-3593.
13. R. F. Bader, *Chemical Reviews*, 1991, **91**, 893-928.